# Replacing conventional brittleness indices determination with new attributes using true hydrofracturing mechanism

Ritesh Kumar Sharma[1], Satinder Chopra[1], and Larry R. Lines[2]


## Abstract

Shale resource plays are associated with low permeability; hence, hydraulic fracturing is required for their stimulation and production. Even though considerable nonuniqueness exists in identifying favorable zones for hydraulic fracturing, geophysicists seem to be avid followers of low-Poisson's ratio and high-Young's modulus brittleness criteria, proposed a decade ago. We highlight the misinterpretation that one may run into in following such a criterion for any shale play and develop a new attribute that makes use of strain energy density and fracture toughness. Although the former controls fracture initiation, the propagation of fractures is governed by the latter. Because hydraulic fracturing comprises both these properties, it is firmly believed that the new proposed attribute could be used to highlight the favorable intervals for fracturing. Core data, well log curves, along with mud logs have been used to authenticate the proposed attribute. Finally, computation of the new attributes is implemented on the seismic data with encouraging results.


## Introduction

Hydraulic fracturing in very low-permeability shale formations enhances the flow of fluids with the propagation of complex fractures through them and is being used for their exploitation. However, the effective propagation of complex fractures is dependent on a rock's ability to fail in a brittle manner. For this reason, pockets in organic shale formations that exhibit higher brittleness are selected for reservoir completion by way of fracturing. One might argue that all rocks should fail in a brittle manner when put under stress, because no ductile behavior in rocks is expected, analogous to metals. However, not all rocks exhibit similar brittle behavior; thus, we need to be able to quantify this property on them. Consequently, different methods have evolved over time that are based on (1) the mechanical properties of rocks, (2) their rock composition, and (3) the use of elastic parameters characterizing the rocks. During the past decade, as shale resource characterization has come to the fore, the term brittleness has become a buzzword. Interestingly, although we look for a way to quantify brittleness of rocks, there is no universally accepted definition or measurement of brittleness, and more than two dozen methods (Jin et al., 2015) have been suggested by different authors under the abovementioned three categories. The underlying assumption in these methods is that a formation with high brittleness is easy to fracture, which is not always true. The methods in categories 1 and 2 above make measurements or carry out analysis on rock samples and use that information to compute a brittleness measure. Methods under category 3 help determine the elastic parameters from seismic data and after appropriate corrections compute a brittleness measure. Because these methods yield spatial distribution of brittleness from 3D seismic data, they are found to be attractive.

At the outset, the elastic parameters that are used in these methods are discussed. Because Poisson's ratio is a measure of the geometric change in shape due to applied stress, or the resistance of a rock against deformation in the lateral and longitudinal directions, it is taken as its strength. Young's modulus is a measure of stiffness of the rock. Both of these parameters are used in the computation of brittleness, among others.

## Determination of elastic parameters

Determination of elastic parameters can be done in different ways. The first types of measurements are those wherein the rock samples are loaded with known stress magnitudes and the resulting strain amplitudes are measured. A typical application of stress on a core sample of the subsurface rock and studying how it fails is called the uniaxial compressive test, in which the two other stresses are zero (Figure 1a). Such a test yields the unconfined compressive strength of the rock, which can easily give away along the planes of weakness in the core sample. A more preferred test is the triaxial

[1]Formerly at TGS, Calgary, Alberta T2P 0R4, Canada. E-mail: riteshpes@gmail.com; satichop@gmail.com (corresponding author).
[2]University of Calgary, Calgary, Alberta T2N 1N4, Canada, deceased.

Manuscript received by the Editor 24 June 2019; revised manuscript received 21 June 2020; published ahead of production 24 June 2020.
This paper appears in *Interpretation*, Vol. 8, No. 4 (November 2020); p. 1–15, 20 FIGS., 2 TABLES.
http://dx.doi.org/10.1190/INT-2019-0103.1. 

compressive test (Figure 1b), wherein confining stress is applied on the core sample and then the axial stress is applied until it fails. While performing such tests, the axial strain is noted as a function of the axial stress and the two are then plotted. Figure 2 shows such a tensile stress-strain curve. The relationship between the applied stress to the resultant strain is given by Hooke's law, which postulates that it is linear. The slope of the linear or straight-line stress-strain curve yields the Young's modulus. The temporary change in shape of the rock samples under applied stress such that it regains its original position once the stress is removed is referred to as elastic deformation. However, because the applied stress is continuously increased, the elastic limit of the rock sample is crossed, so that the straight line deviates into a curved segment exhibiting plastic deformation; that is, rocks undergo permanent deformation when the applied stress is removed. If the rock sample is subjected to more stress loading, it could reach its failure limit, when the rock sample could get ruptured. Depending on their characteristics, rocks are normally classified as either brittle or ductile. These two parameters can be differentiated based on the amount of plastic deformation that the rock undergoes before fracture occurs. Extensive plastic deformation occurs in ductile rocks prior to fracturing, whereas brittle rocks show little or no plastic deformation before they get fractured. Young's modulus or Poisson's ratio calculated from such stress-strain or deformational measurements is referred to as static moduli.

The second type of measurements carried out for the laboratory determination of elastic constants is when velocity is used for their calculation. For example, ultrasonic waves are made to travel through a known length of a rock sample and the corresponding traveltime determined from the first arrival of the compressional wave (P-wave) and shear wave. The Young's modulus and Poisson's ratio computed from these velocities and density are referred to as dynamic moduli. Such dynamic computations could be carried out from sonic log data, as well as seismic surveys; the only difference between the velocities would be their measurements at different frequencies, namely, kilohertz for sonic logs and close to hundred hertz or so for seismic data.

By making ultrasonic measurements in the laboratory on rock samples from the Barnett and deriving the Young's modulus and Poisson's ratio, Rickman et al. (2008) use the average of the normalized Young's modulus and Poisson's ratio and propose the following empirical equation for evaluating brittleness of a rock formation:

$$\mathrm{BI} = 0.5\left\{\left[\frac{E - E_{\min}}{E_{\max} - E_{\min}}\right] + \left[\frac{\nu - \nu_{\max}}{\nu_{\min} - \nu_{\max}}\right]\right\}, \quad (1)$$

where $E$ is the Young's modulus and $\nu$ is the Poisson's ratio. The terms $E_{\min}$ and $E_{\max}$ are the minimum and maximum values of Young's modulus; similarly, $\nu_{\min}$ and $\nu_{\max}$ are the minimum and maximum values of Poisson's ratio. In the above definition, it is being assumed that brittle rocks need less effort to break or fracture and thus Poisson's ratio should be low. To maintain the fractures (i.e., the fractures stay open) the rocks should be associated with high stiffness, or the Young's modulus should be high. Thus, for implementation of equation 1 for finding sweet spots in shale formations, quartz-rich pockets with higher Young's modulus and lower Poisson's ratio are likely to fracture in a brittle manner than clay-rich pockets. This criterion has been used quite often for stimulating shale reservoirs. However, the combination of a high Young's modulus and a low Poisson's ratio as a brittleness measure may not be true for all shale formations because different shale formations exhibit different characteristics based on their mineralogy. It is worth mentioning that Rickman et al.'s (2008) approach works well in which a negative correlation between Young's modulus and Poisson's ratio exists. In a scenario in which a positive correlation between these two properties holds true, it is challenging to select the intervals corresponding to the low Poisson's ratio and high Young's modulus. An example of this behavior of the two parameters is cited from the Montney area in British Columbia, Canada, and a crossplot of the Young's modulus and Poisson's ratio for well data as shown in Figure 3. Notice the positive correlation between these two parameters. When these two are combined as per equation 1, a stationary BI is observed. Based on this BI, it is not possible to differentiate between the upper and lower Montney considering their

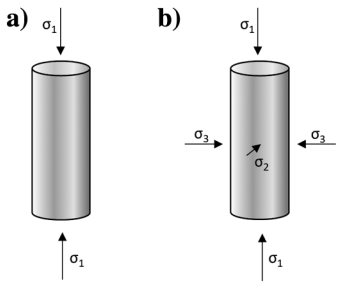


**Figure 1.** Schematic showing application of (a) uniaxial and (b) triaxial stress on rock samples.

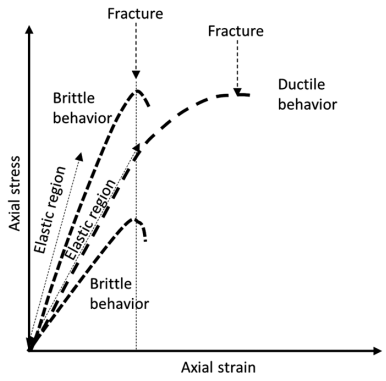


**Figure 2.** Brittle versus ductile behavior of rock samples as seen on a stress-strain graph.

fracturing characteristics. However, it is well known that the upper Montney is favorable for fracturing (McKean, 2017). Thus, a positive relationship of Young's modulus with Poisson's ratio that exists for different unconventional plays (Zhang and Bentley, 2005; Miskimins, 2012; Chopra and Sharma, 2017) makes it difficult for geoscientists to locate favorable drilling zones. Additionally, Rickman et al.'s (2008) proposal received opposition from engineers and geomechanists because they were critical of the very basis of the definition of brittleness used because they thought it was being confused with better fracability. The correlation of high Young's modulus with brittleness gets its main opposition from geomechanics and the engineering domain due to some concerns that are discussed next.

## Brittleness and confining stress

As per geomechanics, when a rock sample of a brittle material is loaded, it can fail in a catastrophic way and has a relatively short plastic deformation in comparison with ductile material. Associating high Young's modulus with brittleness may not always be true as can be understood by considering three different scenarios depicted in Figure 4, which shows that a rock can fail in a brittle manner regardless of the value of the Young's modulus. Further, it is commonly known that rocks deform in a brittle manner at low confining stresses and become ductile beyond a certain level. This conclusion is made based on the experimental works that have been carried out by different researchers (Bai, 2016).

Lutz et al. (2010) study the impact of the confinement of rock brittleness and find that the latter is indeed strongly dependent on the magnitude of confinement. In Figure 4a, the stress-strain curves are shown for four different triaxial tests carried out under different confinement pressures. When the confinement pressure magnitudes are low (1 and 4 MPa), the rock failure appears to be brittle. When pressure magnitudes are increased to 10 MPa, the rock failure becomes ductile,

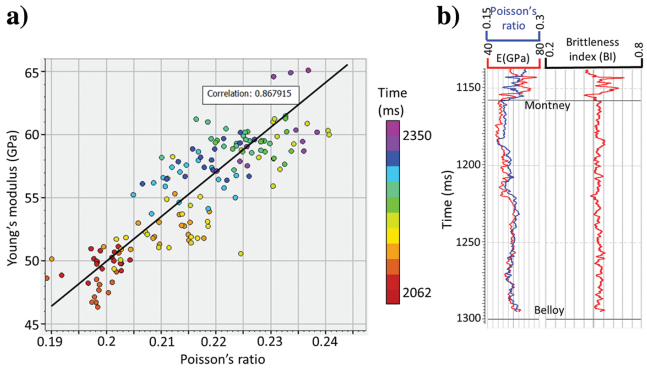


**Figure 3.** (a) Crossplot between Poisson's ratio and Young's modulus for well-log data shown in (b) from the Montney area in British Columbia, Canada. A positive correlation is seen between the two parameters, contrary to Rickman et al.'s (2008) criterion, which leads to an almost-constant linear well BI curve seen in (b).

and there is a slight drop in ductility when the confinement pressure was increased to 20 MPa. With similar experiments conducted for higher strength rocks, all rock failures were found to be brittle in nature, regardless of the significant changes in confinement pressures (109.17–227.29 MPa). Yagiz et al. (2009) also carry out laboratory measurements on six different rock samples and confirm that more brittle rock failure occurs at a lower confinement pressure, whereas ductile failure occurs at higher confinement conditions as shown in Figure 4b. Although higher confinement leads to ductile failure, it is associated with a high Young's modulus, which is contradictory to what Rickman et al. (2008) propose. Realizing such a discrepancy, Holt et al. (2011) make use of elastic and plastic deformation as well as maximum stress ($\tau_{max}$) and residual stress ($\tau_{res}$) parameters (Figure 5a) to propose a new way of estimating the brittleness in terms of brittleness index (BI) as follows:

$$\mathrm{BI} = \frac{\varepsilon_{el}}{\varepsilon_{tot}}, \tag{2}$$

where the total strain ($\varepsilon_{tot} = \varepsilon_{el} + \varepsilon_{pl}$) is the sum of the elastic ($\varepsilon_{el}$) and plastic ($\varepsilon_{pl}$) strains.

To quantify the variation of BI defined by equation 2 as a function of confining stress, the authors carry out triaxial tests on three different shale samples retrieved from different depths in the North Sea and obtain the crossplot shown in Figure 5b. Despite the scatter of the points, the common knowledge about rocks being brittle at low confining stress and vice versa seems to be true and so is the assertion that the stress sensitivity

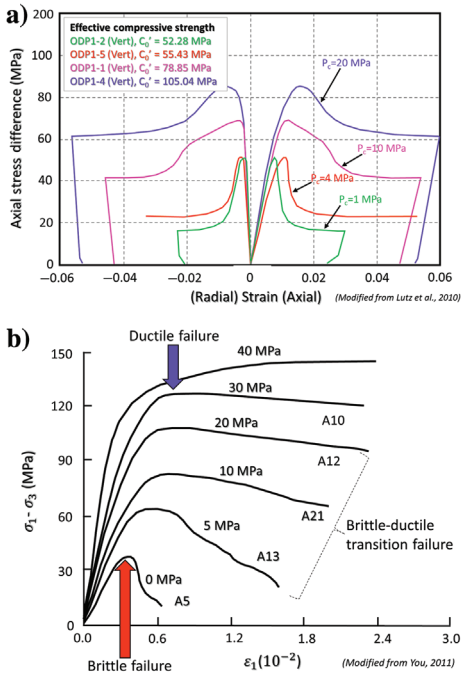


**Figure 4.** Axial stress difference plotted as a function of strain measurements from (a) four and (b) six different triaxial tests (modified from You, 2011).

of brittleness is important and should be considered in its measurement by whatever means. The authors further study the variation of Rickman et al.'s (2008) BI variation as a function of confining stress that is shown in Figure 5c. The BI is seen to be increasing with the increasing confining stress while a negative correlation between them is expected. Before generalizing BI's behavior with confining pressure, it is vital to analyze the impact of the latter on Poisson's ratio also, knowing that Young's modulus follows the confining pressure. By using experimental data from Haynesville Shale in Louisiana, US, and Longmaxi Shale in the southern Sichuan Basin, China, Hu et al. (2015) study the variation of Young's modulus and Poisson's ratio with confining pressure. They conclude that the Young's modulus increases linearly with confining pressure (as expected) for both shales (Figure 6a and 6b). However, no obvious relationship between Poisson's ratio and confining pressure was found as shown in Figure 6b.

## Brittleness and mineral content

The other class of BI computations assumes that a rock's brittleness is related to the abundance of brittle minerals, rather than minerals that are ductile. For example, the presence of quartz mineral in a formation could make it more brittle, whereas more clay content can make it ductile (Jarvie et al., 2007). Later, it was observed that the presence of dolomite tends to increase the brittleness of a shale play (Wang and Gale, 2009). Further, Jin et al. (2015) note that instead of dolomite, the carbonate contribution (dolomite/calcite) should be considered for computation of brittleness. These authors propose a BI for identification of brittle zones in a shale play as follows:

$$\mathrm{BI}_{\mathrm{mineralogy}} = \frac{W_{\mathrm{quartz}} + W_{\mathrm{calcite}} + W_{\mathrm{dolomite}}}{W_{\mathrm{total}}}, \qquad (3)$$

where $W$ corresponds to the weight fraction. Thus, an investigation of different minerals in the zone of interest can lead to the identification of favorable drilling zones. However, the mineralogy-based BI comes with its own problems. Similar results in terms of $\mathrm{BI}_{\mathrm{mineralogy}}$ are obtained even when different weight mineral fractions of quartz, carbonate, and shale are used for its computation as shown in Figure 7. Different combinations of the three minerals will always add up to the same numerator resulting in similar BI values. It would thus be difficult to identify the favorable mineral combinations for fracturing as per the BI computed from mineralogy alone. Also, it is an arduous task to compute the individual mineral content of a formation using seismic data; geoscientists rely on the determination of Young's modulus and Poisson's ratio attributes (Sharma and Chopra, 2015) for its computation. Mathia et al. (2016) make another interesting observation that when a porosity component is introduced in $\mathrm{BI}_{\mathrm{mineralogy}}$ computation, its values remain unchanged for different porosity values. Additionally, as per the above equation, it is not

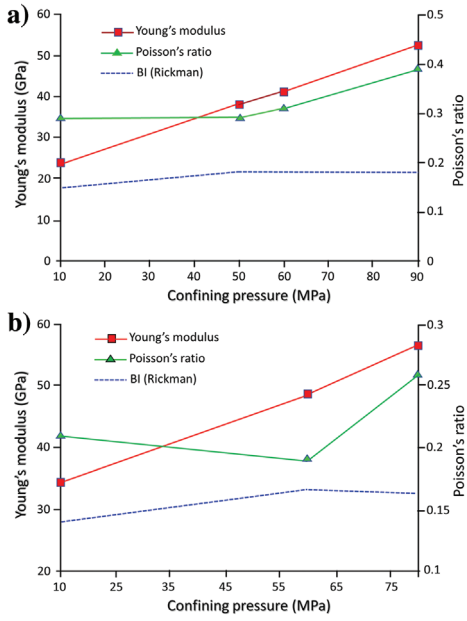


**Figure 6.** Crossplot between the confining pressure and Young's modulus (red) as well as Poisson's ratio (green) for (a) Haynesville shale samples and (b) Longmaxi shale samples. (Modified from Hu et al., 2015.)

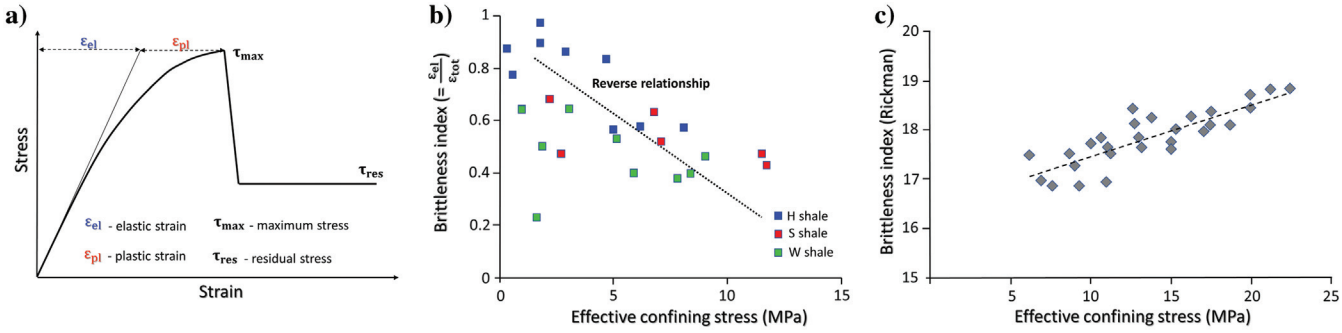


**Figure 5.** (a) A generic crossplot between measured stress and strain depicting how the BI may be estimated. Crossplot between (b) the effective confining stress at failure from triaxial tests on three different shale samples from the North Sea and the BI computed using equation 2. (c) Effective confining stress based on ultrasonic measurements during hydrostatic loading of a shale sample from the North Sea and BI computed using equation 1. (Modified from Holt et al., 2011.)

difficult to conclude that mineralogical BI also does not account for the impact of confining pressure because the same combination of different minerals may exist at different confining pressures. More shortcomings of $BI_{mineralogy}$ computation can be found in Jin et al. (2015) and Hu et al. (2015).

The above discussion can be summarized as follows:

1) Out of the many rock physics elastic moduli available, only Young's modulus and Poisson's ratio are being used in BI computation, which may be insufficient.
2) The normalization of Young's modulus and Poisson's ratio required in equation 1 through the minimum and maximum values is being done in an arbitrary manner and thus may not result in accurate computation of BI.
3) Going back to the basics, one may also point out that the concept of brittleness should be associated with stress because it influences the rock's brittle-to-ductile behavior, and any definition of brittleness should be inclusive of stress in some form. In view of this, the relationship between elastic properties of a rock and its failure under stress may include the confining stress that the rock is under because it has a strong influence on the elastic parameters. Another argument that could be mentioned here is that shale formations are found at different depths and thus would be under different confining pressure and temperature. Any computation of BI, which does not consider the effect of confining pressure, could yield only inaccurate results.
4) The above methods cannot explain why rocks exhibiting high brittleness act as fracture barriers instead of propagating fractures.

Such a discussion points to an important flaw in brittleness computation via Rickman et al.'s (2008) approach and mineralogical approaches in that they ignore the confining stress that the rocks are under at all times and hence ignore the true mechanism of hydraulic fracturing. Therefore, it is advisable to revisit the hydraulic-fracturing process.

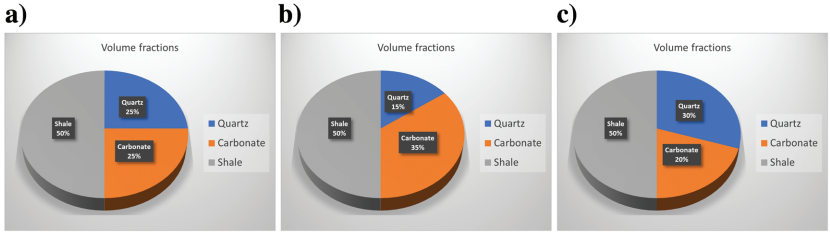


**Figure 7.** Pie charts constructed for different mineral volume fractions yield the same value (0.5) for BI, even though their fracturing responses may be different.

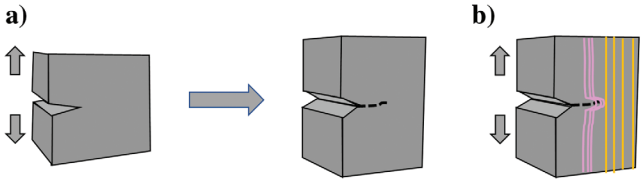


**Figure 8.** (a) Hydraulic fracturing process consists of crack initiation (left) and propagation (right). (b) Fracture initiation disturbs the stress state within the rock due to the stress concentration at the crack tip. (Modified from Rocha-Rangel, 2011.)

## Mechanism of hydraulic fracturing

Let us turn to the basics of hydraulic fracturing of rocks, which entail the initiation of fractures and their propagation as depicted in Figure 8a. To initiate a fracture, priority should be given to a material, which absorbs less energy before it gets fractured. Once the fracture is initiated, the stress state within the rock gets disturbed due to stress concentration at the crack tip as shown in Figure 8b where the yellow vertical lines and red curved lines represent the uniform stress condition and stress concentrate state, respectively. A rock can withstand fracture tip stresses up to a critical value, which is referred to as the critical stress intensity factor; this ability of a rock to resist fracturing and propagation of preexisting fractures is known as fracture toughness (FT). Rocks with low FT promote fracture propagation. Thus, the amount of energy that a formation consumes in the fracture initiation process as well as its FT must be considered in identifying the favorable zones to be fractured. Having said this, now the main challenge is how to estimate them in the geophysical domain. For facilitating this, two terms called strain energy density (SED) and FT are introduced and discussed next.

### SED

When a subsurface rock is being acted upon by fluid injection during hydraulic fracturing, the fluid does work on the rock. This work is stored in the rock in the form of elastic strain energy and comprises components that cause volume changes as well as distortion by way of angular change. Although the normal strains cause a change in volume, the distortion is caused by shear strain.

Following the linear elastic fracture theory, the elastic strain energy per unit volume of isotropic rock is referred to as SED, and for a cube of rock, it is given as (Kelly, 2015)

$$U_{\text{tot}} = \frac{1}{2}(\sigma_x\varepsilon_x + \sigma_y\varepsilon_y + \sigma_z\varepsilon_z + \tau_{xy}\gamma_{xy} + \tau_{xz}\gamma_{xz} + \tau_{yz}\gamma_{yz}), \tag{4}$$

where $\sigma$ is the normal stress; $\varepsilon$ is the equivalent strain; and $\tau$ is the shear stress in the three directions $x$, $y$, and $z$ and is given as follows:

$$\varepsilon_x = \frac{1}{E}[\sigma_x - \gamma(\sigma_y + \sigma_z)],$$
$$\varepsilon_y = \frac{1}{E}[\sigma_y - \gamma(\sigma_x + \sigma_z)],$$
$$\varepsilon_z = \frac{1}{E}[\sigma_z - \gamma(\sigma_y + \sigma_x)],$$

and

$$\tau_{xy} = \mu\gamma_{xy},$$
$$\tau_{xz} = \mu\gamma_{xz},$$
$$\tau_{yz} = \mu\gamma_{yz},$$

where $\mu$ and $\gamma$ are the shear modulus and shear strain, respectively.

Thus,

$$U_{\text{tot}} = \frac{1}{2E}(\sigma_x^2 + \sigma_y^2 + \sigma_z^2) - \frac{\nu}{E}(\sigma_x\sigma_y + \sigma_x\sigma_z + \sigma_y\sigma_z) + \frac{1}{2\mu}(\tau_{xy}^2 + \tau_{xz}^2 + \tau_{yz}^2). \quad (5)$$

Due to the tensile fracture (no shear stress) mode (Jin et al., 2015) in hydraulic fracturing, the last term can be ignored so that

$$U_{\text{tot}_{\text{HF}}} = \frac{1}{2E}(\sigma_x^2 + \sigma_y^2 + \sigma_z^2) - \frac{\nu}{E}(\sigma_x\sigma_y + \sigma_x\sigma_z + \sigma_y\sigma_z). \quad (6)$$

The above equation shows that the amount of energy required to initiate a fracture is a function of Young's modulus, Poisson's ratio, and the principal stresses. Although computation of the first two parameters from seismic data is straightforward, determination of the latter could be challenging. This difficulty could stem from the fact that the three principal subsurface stresses may be unequal, and their measurement using seismic data would be an arduous task. Thus, for getting some insight into SED and its estimation, one could make some assumptions to simplify the analysis. One such simplification is to take the horizontal stresses to be equal in magnitude and correlated with the vertical stress through the Poisson's ratio. The hydrostatic condition simplifies the above equation further and is considered here. The resulting equation yields the SED in terms of Young's modulus ($E$), Poisson's ratio ($\nu$), and the confining pressure, which can then be determined from well or seismic data. It may be appropriately mentioned here that the above elastic parameter determination is dynamic in nature and would need to be calibrated for obtaining the static versions.

## FT

FT can be determined in different ways: direct and indirect. The direct way is to perform measurements on rock samples, which is more difficult and complex than other tests of rock mechanical properties. Therefore, a correlation of FT with Young's modulus, Poisson's ratio, tensile strength, and compressive strength (CS) has been derived from experimental data of different types of rocks (Barry et al., 1992). Sierra et al. (2010) publish experimental data showing the relationship between FT and tensile strength, CS, Young's modulus, and Poisson's ratio for the Woodford shale.

That rocks resist the propagation of preexisting cracks is common knowledge, a minimum pressure is required to overcome this resistance and make a fracture grow. Thus, the minimum pressure required to grow the fracture can be correlated with FT because the higher the FT, the higher the required minimum pressure will be. If somehow this pressure is estimated, it can be used as a proxy for FT. There are two different ways that FT could be estimated in the geophysical domain. One way is to use its relationship with the P-wave velocity and Young's modulus as published and then take their optimal combination (the root-mean-square average, arithmetic mean, etc.). The second way is to estimate the minimum pressure required for fracture propagation. Based on the theory proposed by Griffith (1920, 1924) to explain the rupture of brittle, elastic material, Sack (1946) derives an equation to predict the minimum pressure (critical) necessary to extend a fracture in a rock for hydraulic fracturing considering the penny-shaped cracks as

$$P_c = \sqrt{\frac{\pi\alpha E}{2(1-\upsilon^2)C}}, \quad (7)$$

where α is the specific surface energy of the rock and $C$ is the crack length. A relevant assumption about the crack length simplifies the above equation to yield the critical pressure per unit volume of fracture and allows us to compute it using well log data or seismic data.

## Synthesis of a new attribute

Now that the SED, which is a measure of the energy absorbed by the formation before fracturing, and FT have been described, a new attribute is framed for which we have coined the term hydraulic fracturing coefficient (HFC). It is computed as the average of the normalized SED and normalized FT and written as

$$\text{HFC} = \frac{1}{2}(\text{SED}_{\text{norm}} + \text{FT}_{\text{norm}}), \quad (8)$$

where $\text{SED}_{\text{norm}} = \frac{\text{SED}_{\text{max}} - \text{SED}}{\text{SED}_{\text{max}} - \text{SED}_{\text{min}}}$ and $\text{FT}_{\text{norm}} = \frac{\text{FT}_{\text{max}} - \text{FT}}{\text{FT}_{\text{max}} - \text{FT}_{\text{min}}}$.

With the new attribute proposed, the next task is to validate it as a measure of fracability. For doing so, the experimental data available in the literature are used and application of HFC is illustrated by comparing it with the CS of a material. Thereafter, well-log data from the Delaware Basin are used to compute HFC, which then assisted in identifying the favorable zones for hydraulic fracturing. The processed mud log available for one well helps in supporting the interpretation of pref-

erable zones to be fractured hydraulically. The Appalachian Basin well-log data are used next to validate HFC as a measure of fracability using X-ray diffraction (XRD) data as well as petrographic results. The details of the validation process are discussed as follows.

### Validation of HFC as a measure of fracability

*Using experimental data:* To validate the proposed attribute, the experimental data published by Hu et al. (2015) are used, wherein the uniaxial compression test, scanning electron microscope, and XRD methods have been analyzed to obtain the mechanical properties, texture, and crack characteristics of rocks collected from different regions. The test results were given in terms of Young's modulus, Poisson's ratio, confining pressure, CS, peak strain, and residual strain for data samples from the Haynesville Shale, Eagle Ford Shale, Barnett Shale, and Longmaxi Shale. The parameters of interest are shown in Table 1, where, as expected, a strong positive correlation of confining pressure with CS is evident. With access to these parameters, it is easy to compute $BI_{Rickman}$ and HFC. Because it is well known that a material with higher strength is not easy to fracture, its CS can be treated as a measure of fracability. Therefore, HFC and $BI_{Rickman}$ are crossplotted with the CS as shown in Figure 9a and 9b to authenticate their applicability for highlighting the favorable zones for fracturing. As per its definition, an inverse linear relationship between CS and an indicator of fracability is anticipated. However, a positive linear relationship is seen between CS and $BI_{Rickman}$. This behavior is because Young's modulus increases with the increasing confining pressure, although the impact of the confining pressure on Poisson's ratio is not clear. Consequently, $BI_{Rickman}$ cannot be treated as an indicator of fracability. The HFC, however, exhibits a decreasing trend with the increasing CS. Thus, it can be concluded that the proposed attribute accounts for the impact of strength on the fracability analysis in a proper way. Further, considering the published results of Hu et al. (2015) and the available XRD data as shown in Table 2, HFC, $BI_{mineral}$, and $BI_{Rickman}$ were computed. Thereafter, they were crossplotted with CS as shown in Figure 10 for checking their relevancy in hydraulic-fracturing analysis. Again, $BI_{mineral}$ and $BI_{Rickman}$ show an increasing trend with CS, whereas HFC shows a decreasing trend, as expected. The inverse linear trend noticed between HFC and CS of the rock samples from different unconventional plays lends confidence in its applicability for hydraulic-fracturing analysis.

### Applications using well log data
### *From the Delaware Basin, USA*

To implement the proposed attribute on real data, the dipole sonic and density log curves for a well from the Delaware Basin were picked up, where the zone of interest is from the Bone Spring Formation to the Mississippian Formation. First, the Young's modulus and Poisson's ratio using well-log curves are computed and crossplotted as shown in Figure 11. Although the shallow interval from Bone Spring to Wolfcamp exhibits a positive trend (the blue ellipse), a mixed trend is noticed over an interval from Wolfcamp to Mississippian (the red and cyan ellipses). Evidently, it is challenging to identify the favorable zones for fracturing based on the Rickman et al. (2008) criteria.

To overcome this problem, a crossplot of SED and FT is generated using well-log data as shown in Figure 12a. The cluster points exhibit a nonlinear trend, which is analogous to the one typically seen on P-impedance versus $V_P/V_S$ crossplots. Clusters of data points with different combinations of SED and FT have been enclosed in colored ellipses and back-projected onto the well-log curves shown in Figure 12b. It is noticed that the shallow interval from Bone Spring to Wolfcamp exhibits high FT and low SED and the deeper interval for Barnett Shale is associated with an opposite combination. Low SED and high FT

**Table 1. Experimental data given in Table 3.2 of Hu et al. (2015) in terms of elastic parameters along with confining pressure and CS.**

| Confining pressure (MPa) | Young's modulus (GPa) | Poisson's ratio | CS (MPa) |
|---|---|---|---|
| 90 | 52.61 | 0.39 | 209.19 |
| 60 | 41.4 | 0.31 | 171.92 |
| 50 | 38.15 | 0.29 | 143.73 |
| 10 | 23.73 | 0.29 | 42.3 |
| 10 | 12.13 | 0.29 | 35 |
| 10 | 25.43 | 0.35 | 42.49 |
| 50 | 34.74 | 0.27 | 214.09 |
| 30 | 20.91 | 0.21 | 40.57 |
| 20 | 19.56 | 0.48 | 40.56 |
| 30 | 14.33 | 0.21 | 37.75 |
| 60 | 70.4 | 0.41 | 391.25 |
| 80 | 56.58 | 0.26 | 215.13 |
| 60 | 48.54 | 0.19 | 210.17 |
| 15 | 34.48 | 0.21 | 78.5 |

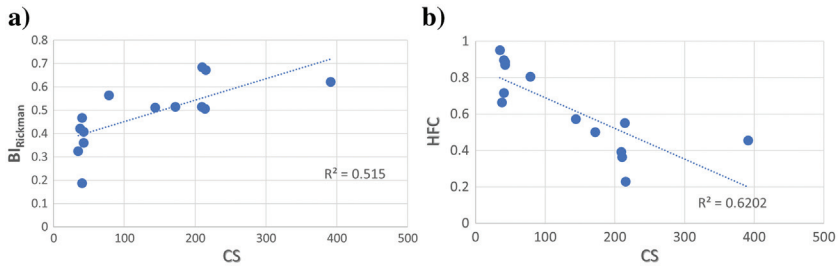


**Figure 9.** Crossplots between (a) $BI_{Rickman}$ and CS and (b) HFC and CS. (Data from Hu et al., 2015.)

values imply that the interval is amenable to fracture initiation but not to propagation.

That low values of SED signify less energy for fracture initiation noticed in the shallower interval is supported by the lower strength of the formations expected at shallow levels, which tends to increase with depth. Previous studies (Bowker, 2007; Miller et al., 2013) have demonstrated that the fracture initiation pressure (represented by SED) increases linearly with the increase in clay content — being high for clay-rich zones and low for clay-lean zones. Because the mud log (Figure 12b) indicates an abundance of carbonate and a small amount of clay in the Bone Spring to the top Wolfcamp interval, it must be associated with low values of fracture initiation pressure, which is supported by the observed low SED values.

Different authors (Wang and Carr, 2012; Sharma et al., 2018) conclude that clay content alone should not be the only adopted criterion for identification of favorable zones for hydraulic fracturing. These authors emphasize the fact that carbonate content of only up to 40% in the formation offers suitable conditions for hydraulic fracturing. Thus, for formations with carbonate content of greater than 40%, there will be resistance to fracture propagation and such formations would act more as fracture barriers. Consequently, high values of FT would be expected for the Bone Spring to top Wolfcamp interval.

In a similar vein, for the deeper clay-rich Barnett to Mississippian interval, the higher confining pressure increases the strength of the formation; thus, it would be associated with high values of SED and low values of FT. This implies that this interval should absorb more energy before the initiation of hydraulic fractures.

Considering that fracture initiation and propagation are important for hydraulic fracturing, combinations of low SED and high FT or high SED and low FT may not be suitable for fracturing. Both of these combinations lead to low values of an indicator of fracability such as HFC and are shown alongside the SED and FT curves

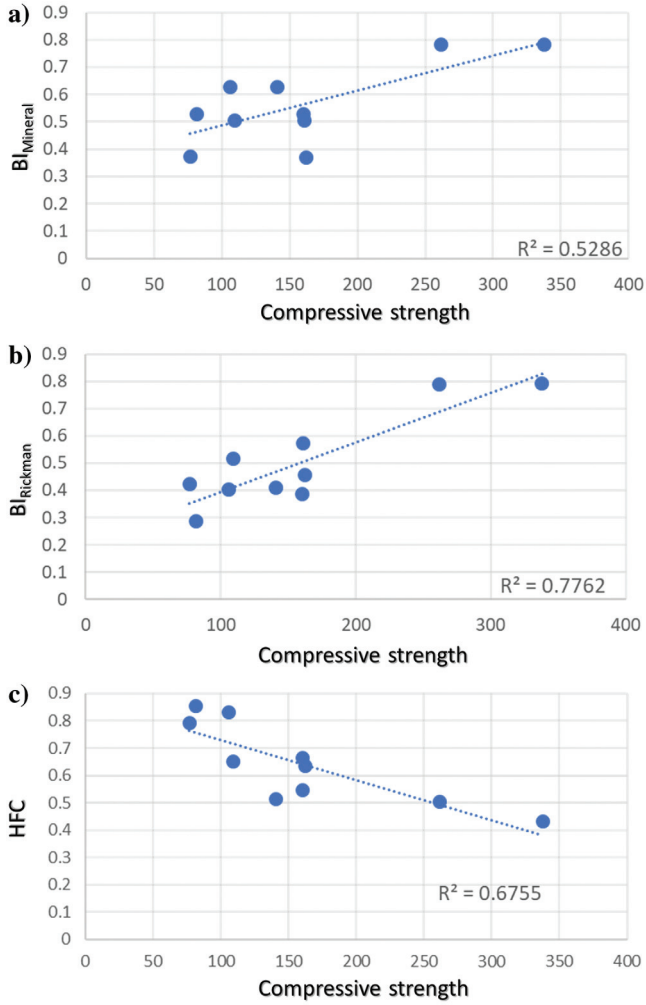


**Figure 10.** Crossplots between CS and (a) $BI_{mineral}$, (b) $BI_{Rickman}$, and (c) HFC. Notice that the brittleness indices in (a and b) show an increasing trend but HFC shows a decreasing trend in (c), which is as per our expectation.

**Table 2. Experimental data given in Table 3.1 of Hu et al. (2015) in terms of elastic parameters along with confining pressure, CS, and brittle mineral content.**

| Brittle mineral (%) | Clay (%) | Confining pressure (MPa) | CS (MPa) | Young's modulus (GPa) | $BI_{Rickman}$ |
|---|---|---|---|---|---|
| 78.2 | 16.17 | 15 | 261.77 | 31.6 | 0.789 |
| 78.2 | 16.17 | 30 | 337.87 | 31.5 | 0.791 |
| 62.6 | 35.35 | 15 | 105.95 | 6.6 | 0.403 |
| 62.6 | 35.35 | 30 | 140.71 | 7.5 | 0.409 |
| 50.55 | 43.41 | 15 | 109.535 | 21.8 | 0.517 |
| 50.55 | 43.41 | 30 | 160.815 | 23.8 | 0.572 |
| 52.75 | 39.86 | 15 | 81.73 | 4.9 | 0.286 |
| 52.75 | 39.86 | 30 | 160.215 | 12.5 | 0.385 |
| 37.1 | 42.8 | 15 | 76.86 | 12.78 | 0.422 |
| 36.8 | 46.9 | 30 | 162.33 | 16.73 | 0.456 |

in Figure 12b. Higher values of HFC are more appealing and come from an optimal combination of FT and SED. In Figure 12a, such a combination is observed for an interval within the Wolfcamp (the green ellipse in Figure 12a), which is essentially a limey shale as seen in the mud-log strip.

As an important conclusion from the above exercise, a small proportion of limestone within the shale offers a suitable condition for fracture initiation and propagation. This matches well with the results of previous studies, in which formations with clay content less than 50% as well as carbonate content not more than 40% are preferable for hydraulic fracturing (Miller et al., 2013; Sharma et al., 2018). Needless to mention, this interval has been stimulated heavily for production.

### *From the Appalachian Basin, USA*

Being encouraged with the results observed in the Delaware Basin, well log data (dipole sonic and density) from the Appalachian Basin are considered next where the Utica play is of interest. The primary target zone in the Utica play includes the basal Utica, an organic calcareous shale; Point Pleasant, an organic-rich carbonate interbedded with calcareous shale that underlies Utica; and the upper Trenton of the Black River group, an organic-rich carbonate that underlies Point Pleasant. The three zones represent a transgressive system tract, in which the shallow shelf carbonates of the Trenton were cyclically flooded by rising seas. To begin with, Young's modulus and Poisson's ratio are computed using well-log curves and displayed together as shown in Figure 13a. It is noticed that these two curves are following each other over the Point Pleasant to Trenton interval. Given the positive relationship between Young's modulus and Poisson's ratio, the applicability of the Rickman et al. (2008) criteria for identifying the favorable zones to be fractured in the Utica play is questionable because data points yielding a low Poisson's ratio and a high Young's modulus are difficult to enclose on their crossplot shown in Figure 13b.

Next, SED and FT are computed using well-log data and crossplotted together as shown in Figure 14a. Again, a nonlinear trend of cluster points similar to the one observed in the Delaware basin is noticed. Clusters of data points with different combinations of SED and FT have been enclosed in colored ellipses and back-projected on the well log curves shown in Figure 14b. It is not difficult to conclude that the data points associated with the Utica Formation exhibit the best combination of SED and FT because high values of HFC are noticed over this interval as shown on the right track of Figure 14b. Because high values of FT and low values of SED are noticed for the Trenton interval, it can be stated that this interval is favorable for fracture initiation but not for propagation, whereas the Point Pleasant interval offers preferable conditions to fracture propagation because low val-

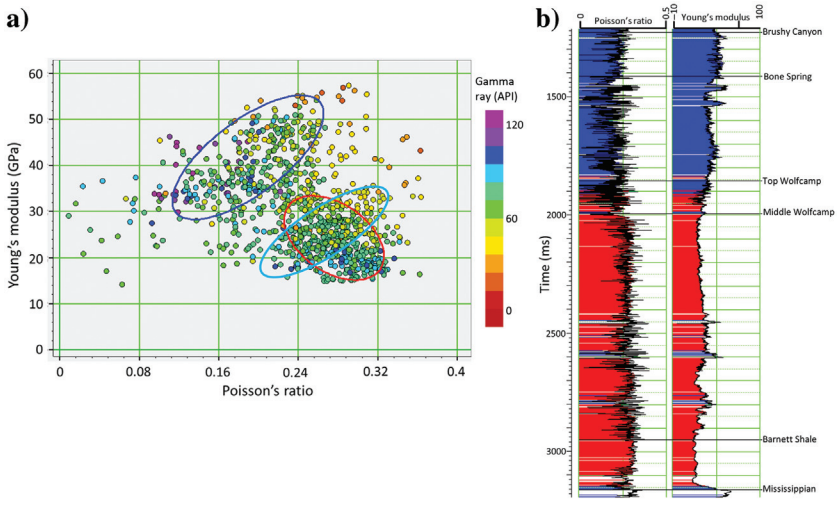


**Figure 11.** (a) Crossplot between Young's modulus and Poisson's ratio for well-log data from the Delaware Basin. (b) Back projection of cluster points within different colored polygons onto the well curves. The different trends seen on this crossplot make it challenging to identify the fracturing zones in the zones of interest. Although a positive correlation is seen for the shallow interval, a mixed type of correlation is noticed for the deeper zone as shown in (b).

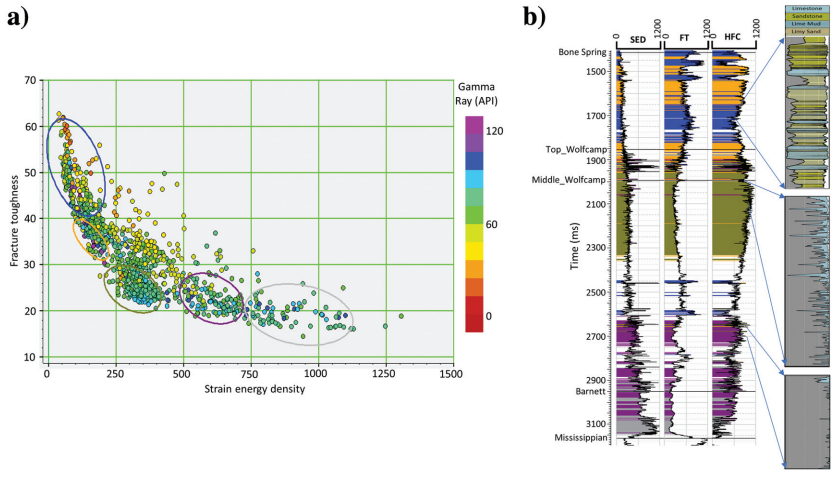


**Figure 12.** Crossplot between SED and FT for well data within the Bone Spring and Mississippian geologic markers. Different clusters of data points corresponding to different combinations of SED and FT have been picked and back-projected onto the computed well log curves for SED, FT, and HFC as shown in (b). The lithostrip as interpreted from the mud log also is shown to the right.

ues of FT are seen. On examining the HFC curve closely, it can be concluded that the lower Point Pleasant is good for fracturing because it yields relatively high values of HFC.

To understand the interpretation of this crossplot, the XRD and regional petrophysical modeling available for the data set at hand are used. As per the XRD data set, quartz, calcite, and clay are the main minerals present in the Utica play. Additionally, regional petrophysical modeling carried out for the condensate region over which seismic data were acquired reveals a strong relationship of clay volume ($V_{clay}$) with the neutron-porosity minus density-porosity (NMD) data. Furthermore, the quartz group (quartz + feldspar) and the carbonate group (calcite + dolomite) showed a strong relationship with the neutron porosity curve (NPHI), as shown in Figure 15. Therefore, the mineralogical content of the Utica play can be obtained if the neutron-porosity (NPHI) and density-porosity (DPHI) are available. Because the NPHI and DPHI curves were available for the considered well, the mineralogical content was computed in terms of $V_{clay}$, $V_{quartz}$ (volume of quartz), and $V_{carbonate}$ (volume of carbonate). Furthermore, the $V_{clay}$ and $V_{carbonate}$ were compared with the one obtained from the XRD as shown in Figure 16 to authenticate the results of regional modeling. A reasonable match noticed between the volume fraction of individual minerals computed using regional petrophysical modeling (the continuous curve) and the XRD data (the tadpole plot) demonstrates that the regional petrophysical modeling can be trusted in determining the mineralogical content for the data set at hand. Once reliable estimation of the individual mineral's fraction is obtained, the crossplots between SED and FT are shown in Figure 17 and are colored coded with them in addition to the total porosity computed by averaging the NPHI and DPHI values. It may be clarified that the volume fraction of clay and quartz varies from 0% to 30% over our zone of interest (the Utica, Point Pleasant, and Trenton intervals), but the volume fraction of carbonate varies from 20% to 90%; thus, it has a greater impact on the fracability. However, the volume fraction of clay is relatively high in the Utica Formation, though less than 40%; thus, it may not have a significant effect on fracability. The presence of the lower content of carbonate in the Utica along with the higher content of quartz and porosity makes it stand out as a favorable candidate for fracturing. The existence of a higher content (>60%) of carbonate in the Trenton Formation makes this interval more resistive to fracture propagation and preferable to fracture initiation. Lower Point Pleasant is more likely to get fractured than upper Point Pleasant based on the HFC values, which include the optimal combination of SED and FT.

Having gained confidence in the applicability of HFC for defining the fracability, seismic data from these two basins were considered next for mapping the lateral fracability in the intervals of interest.

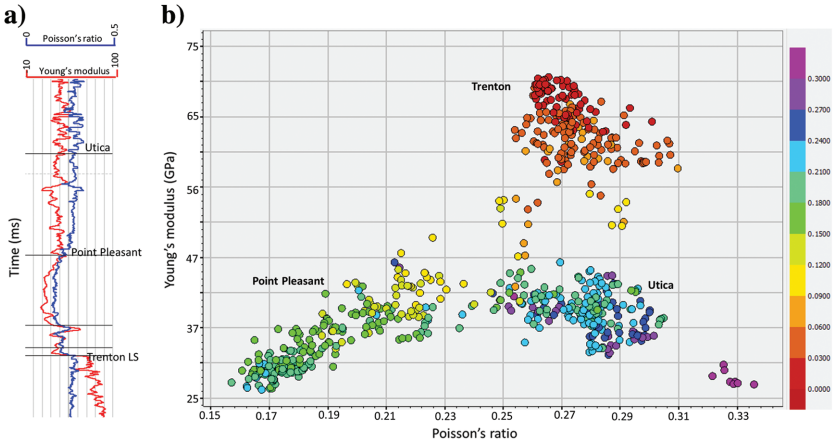


**Figure 13.** (a) Display of the Young's modulus and Poisson's ratio well log curves from the Appalachian Basin and (b) their crossplot color coded with the volume of clay. Although the Point Pleasant and Trenton intervals exhibit positive trends, a negative trend is noticed for the Utica interval. Consequently, it is challenging to follow the Rickman et al. (2008) criterion for identifying the favorable interval to be fractured.

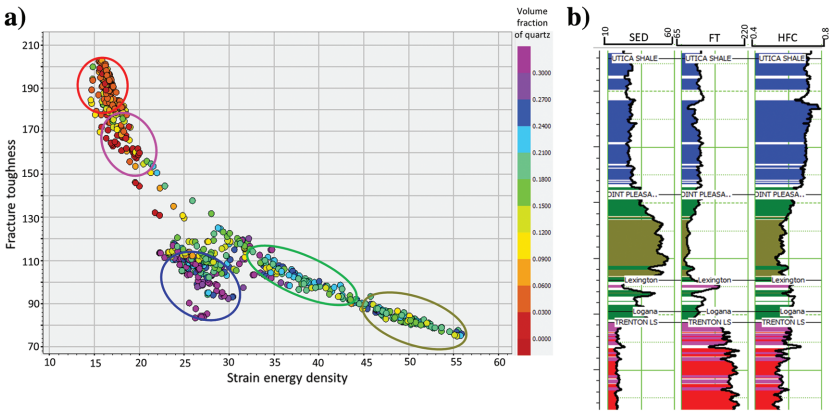


**Figure 14.** (a) Crossplot between SED and FT for well data within the Utica and Trenton limestone geologic markers. Different clusters of data points corresponding to different combinations of SED and FT have been picked and back-projected onto the well log curves as shown in (b). The Utica shale exhibits the best combination of the crossplotted attributes desired for identifying preferable zones for hydraulic fracturing.

## Challenges in estimation of HFC from seismic data

It follows from equations 6 to 8 above that HFC requires the availability of Young's modulus for its computation.

However, estimation of Young's modulus from seismic data involves density, and the extraction of density from seismic data is challenging. To overcome this problem, a new attribute ($E_\rho$) in the form of a product of Young's modulus and density was proposed some time back (Sharma and Chopra, 2015) as given below

$$E\rho = I_S^2\left(\frac{3I_P^2 - 4I_S^2}{I_P^2 - I_S^2}\right). \quad (9)$$

Often, it has been observed that if we compare the computed $E_\rho$ curve from well-log data as well as seismic data with the computed $E$, they look very similar (Sharma and Chopra, 2015). The importance of $E_\rho$ is due to the fact that it is a function of P-impedance and S-impedance, which can be derived from prestack seismic data using simultaneous inversion. Therefore, instead of Young's modulus, $E_\rho$ will be used for HFC estimation.

## Applications using seismic data

*From the Delaware Basin*: Consequently, access was available to all the parameters required for estimating HFC volume from seismic data, except the equivalent 3D volume for confining pressure. To compute it, the density curve was integrated first at different well locations and then propagated with the interpreted horizons over the considered 3D area. Now with the availability of all the required parameters, the HFC volume was obtained. Figure 18a shows the HFC section along an arbitrary line passing through different wells, where high values of HFC are represented by the hot colors. Gamma-ray curves have been overlaid on the section in black. It is noticed that the fracability in Bone Spring decreases as we go from the western to the eastern side of the line. To support this observation, the equivalent 3D seismic facies volume generated using Bayesian classification is shown in Figure 18b. Notice the lowering of fracability observed on the eastern side of the arbitrary line within the Bone Spring Formation, which is consistent with the interpretation of facies volume where an abundance of carbonate content is noticed.

On examining Figure 18a and 18b simultaneously, it can be stated that the individual facies of the Wolfcamp and Barnett intervals such as limey shale, shaly limestone, and clay-rich shale exhibit consistency on going from one side to another, although variation in the fracability exists. It is evident from the figures that although

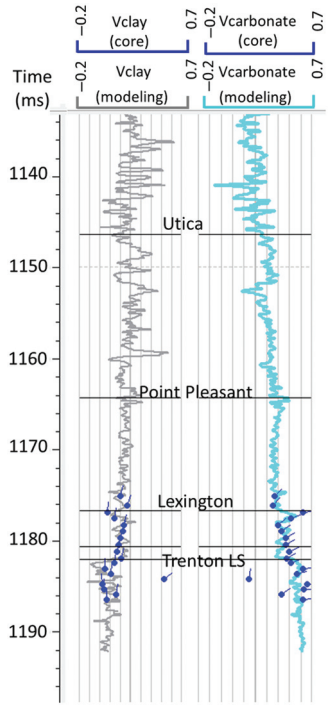


**Figure 16.** A comparison of petrophysical modeling results (the continuous curve) with XRD data (the tadpole plot, the left track) for the volume of clay (the right track) volume of carbonate. A reasonable match is noticed between them, lending confidence in the modeling.

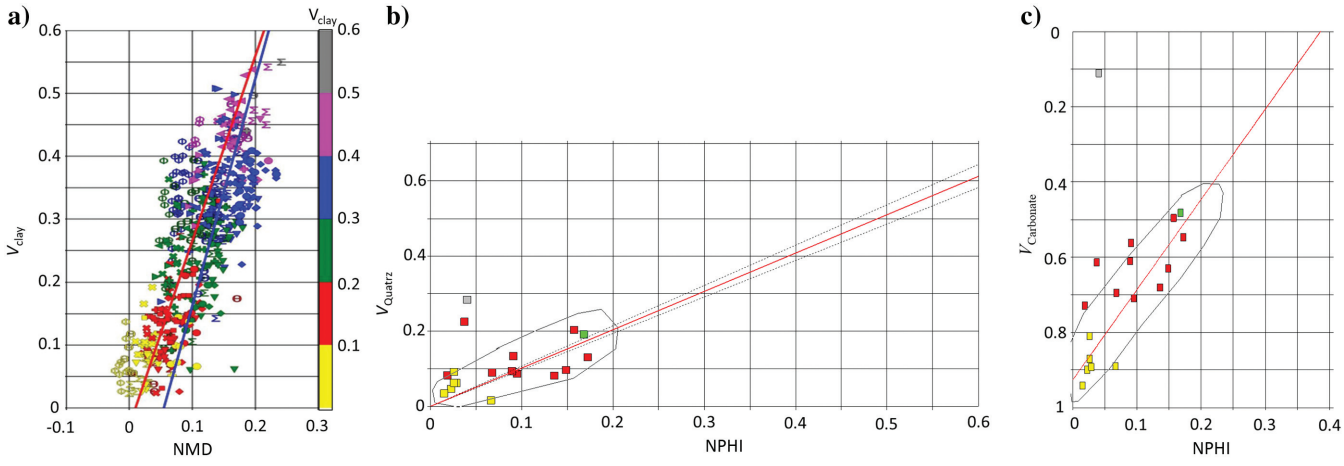


**Figure 15.** Petrophysical modeling reveals a strong relationship among (a) NMD and the volume of clay, (b) NPHI and the volume of quartz group, and (c) NPHI and the volume of carbonate group. The data points are all color-coded with the volume of clay as exhibited in panel (a) (Sharma and Chopra, 2018).

the eastern side of individual formations offers better conditions to hydraulic fracturing (the magenta ellipses), poor conditions are noticed on the western side of the line (the brown ellipses). This observation is justifiable in view of the impact of confining pressure on the fracturing conditions, which is anticipated to be higher over the western side of the line. The matching of carbonate stringer (the gray block arrow to the right) with lower values of HFC within the Wolfcamp interval is convincing because this stringer is expected to act like a fracture barrier at this depth. The matching of the interpretation carried on these two sections obtained by following different approaches lends confidence to the applicability of HFC on seismic data.

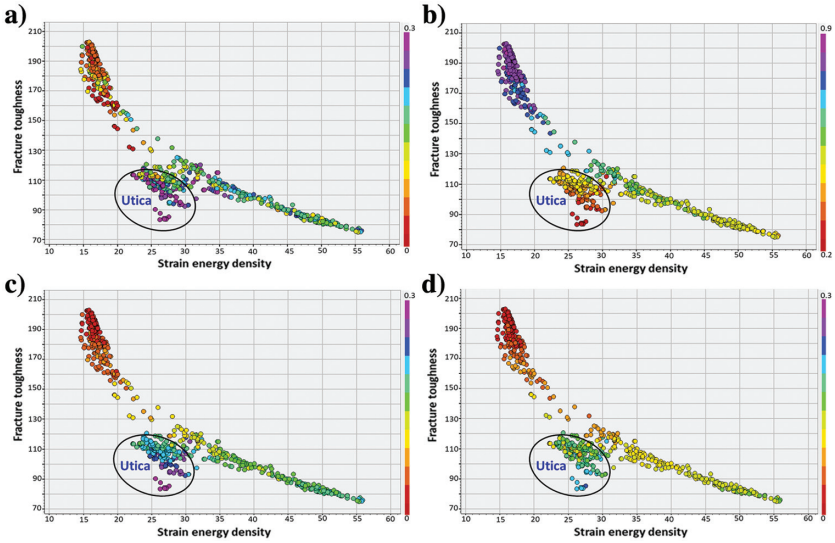


**Figure 17.** Crossplot between SED and FT for well data over an interval from the Utica to Trenton limestone geologic markers, color coded with (a) $V_{clay}$, (b) $V_{carbonate}$, (c) $V_{quartz}$, and (d) total porosity. Notice that the data points corresponding to the Utica Formation exhibit an optimal combination (< 50% clay and < 40% carbonate) of different mineral constituents along with high porosity.

*From the Appalachian Basin:* Being convinced with the application of FT and SED in highlighting the favorable zone for fracturing at the well location and discussed earlier, similar computations were applied to the seismic data from that area. A proper workflow of running simultaneous inversion was followed to extract the desired attributes to determine SED, FT, and hence HFC. Figure 19 shows a section from the HFC volume along an arbitrary line passing through different wells. Notice the Utica as well as the lower Point Pleasant Formations exhibit high values of HFC. Additionally, low values of HFC are noticed in the Trenton Formation, as expected, due to the high amount of carbonate content in this formation. Be-

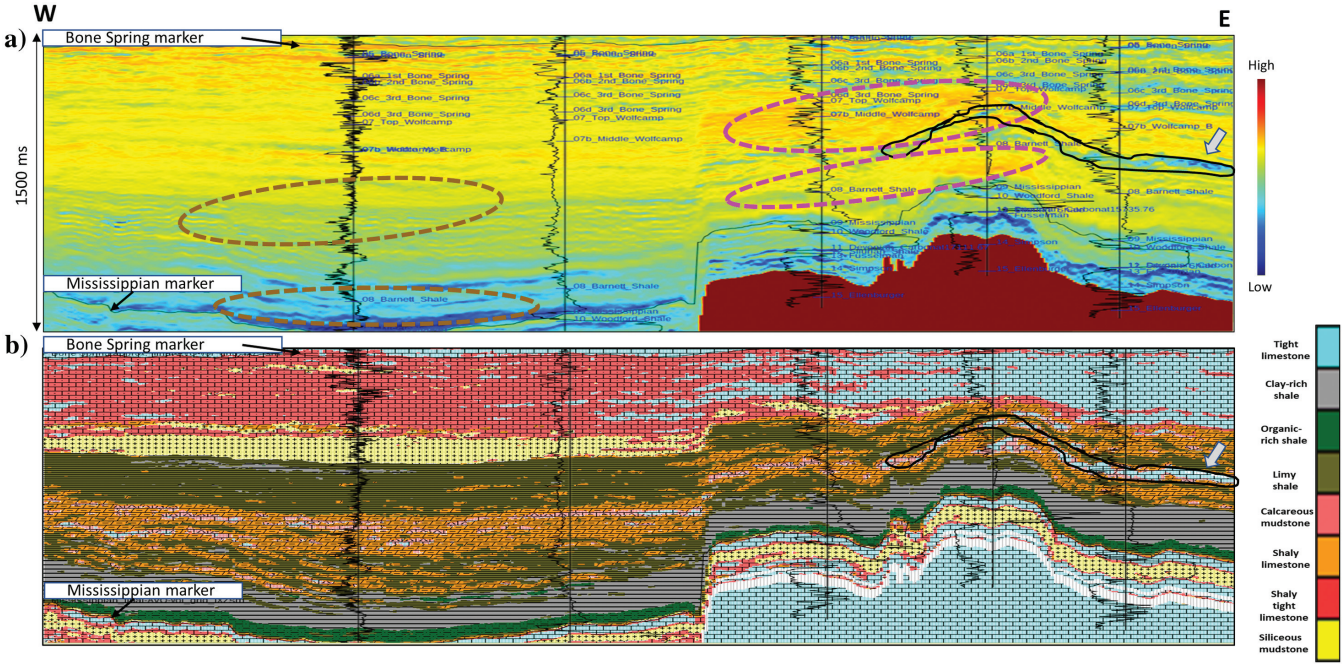


**Figure 18.** An arbitrary line passing through different wells extracted from the (a) HFC volume and (b) lithofacies volume. Gamma-ray curves have been overlaid on the section. The fracability variation noticed laterally within the Bone Spring is supported by the facies volume because the high content of carbonate suggests low fracability on the eastern side. Similarly, the variation of fracability noticed in the individual intervals (the ellipses and polygons) can be correlated again with the facies volume derived independently using Bayesian classification (Sharma et al., 2019) and the concept of confining pressure. (Data courtesy TGS, Houston.)

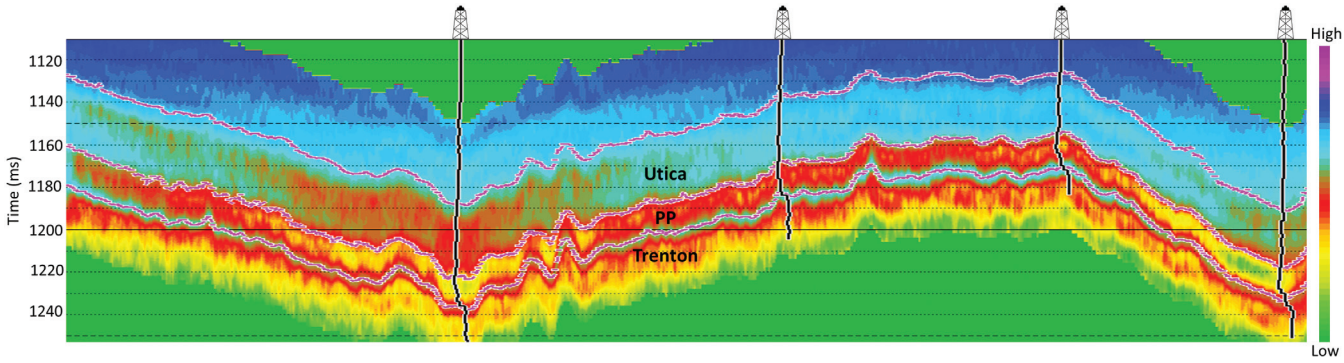


**Figure 19.** An arbitrary line passing through different wells extracted from the HFC volume generated using SED and FT volumes. Fracability variation is seen vertically and spatially within the individual intervals (Utica, Point Pleasant [PP], and Trenton) as annotated. (Data courtesy TGS, Houston.)

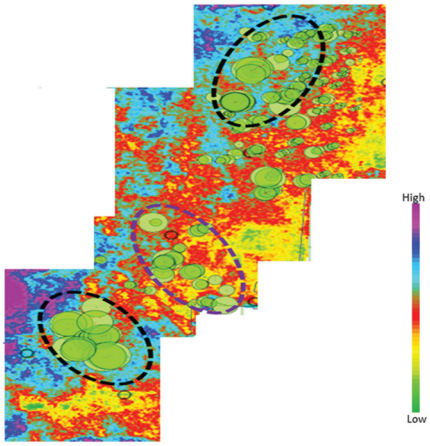


**Figure 20.** A horizon slice extracted from the computed HFC volume (averaged over the lower Point Pleasant interval). Lower fracability zones are indicated by the green and yellow colors, whereas the blue and magenta colors represent higher fracability zones, which qualitatively match the available production data (the green bubbles) over the zones enclosed by the black ellipses. (Data courtesy TGS, Houston.)

cause lower Point Pleasant is the formation of interest, the lateral variation of HFC over this interval is mapped to identify favorable pockets for hydraulic fracturing. Figure 20 shows a horizon slice from the HFC volume computed over a 10 ms window in the lower Point Pleasant interval. The hot colors represent the higher values of HFC and delineate the preferable zones to be fractured. In view of the fact that better hydraulic fracturing leads to better production, six months of oil production data (available in the open database) are overlaid on the HFC display.

It is quite evident that many wells that fall over pockets exhibiting high values of HFC (the black ellipses) are more productive (the size of the bubbles). There are some wells that sit on areas with moderate values of HFC (the purple ellipse) and are somewhat less productive. Both of these observations are encouraging but have been made in a qualitative way for a few reasons, realizing fully well that a quantitative analysis would be more desirable. The first reason has to do with the fact that the production data accessed from the open database do not specify the zones within the multilevel Wolfcamp Formation, wherefrom the production has been recorded. The display shown in Figure 20 is a representative Wolfcamp B level horizon slice on which the production from the whole Wolfcamp Formation is overlaid. If the exact production zones were known, a quantitative analysis could have been carried out in the form of crossplots of HFC versus production in specific zones. Second, production data always are provided in the depth domain, whereas the displayed horizon (Figure 20) is in the time domain. Consequently, it would be difficult to ascertain that the production data overlaid corresponds to the relevant time interval. This problem could be averted by transforming HFC data to the depth domain and then repeating our analysis, which was beyond the scope of the present exercise. Finally, the production data from any well are not only a function of fracability but depend on an optimal combination of different attributes such as porosity, organic richness, and natural as well as induced fractures (Ouenes, 2014). Therefore, expecting a perfect match of well production data with fracability may be an overambitious task entailing uncertainty in the absence of information on the factors stated above.

Thus, considering the limitations under which the above exercise was performed, we firmly believe that the proposed HFC attribute is a good replacement for the conventional brittleness indices being used for characterizing shale formations.

## Conclusion

The different methods of brittleness determination being used in industry, while applicable to certain subsurface rock formations, are not suitable for others. We have pointed out the shortcomings of some of these methods, and then we went on to describe a new attribute that we call HFC that makes use of FT and SED. The proposed attribute was authenticated by using core data, XRD data, along with other data sets. The application of HFC on the well log data as well as seismic

data from the Delaware Basin and the Appalachian Basin has been demonstrated by comparing its interpretation with mud-log data, petrophysical data, and production data.


## Acknowledgments

We wish to thank TGS for encouraging this work and for the permission to present and publish it. The well data used in this work were obtained from the TGS Well Data Library and is gratefully acknowledged.


## Data and materials availability

Data associated with this research are confidential and cannot be released.

## References


Bai, M., 2016, Why are brittleness and fracability not equivalent in designing hydraulic fracturing in tight shale gas reservoirs: Petroleum, **2**, 1–19, doi: 10.1016/j.petlm.2016.01.001.

Barry, N., N. R. Whittaker, and S. G. Singh, 1992, Rock fracture mechanics principles design and applications: Elsevier

Bowker, K. A., 2007, Barnett shale gas production, Fort Worth Basin: Issues and discussion: AAPG Bulletin, **91**, 523–533, doi: 10.1306/06190606018.

Chopra, S., and R. K. Sharma, 2017, Misconceptions about brittleness, and the talk about fracture toughness: AAPG Explorer, 20–21, August issue.

Griffith, A. A., 1920, The phenomena of rupture and flow in solids: Philosophical Transactions of the Royal Society of London. Series A, Containing Papers of a Mathematical or Physical Character, **221**, 163–198.

Griffith, A. A., 1924, The theory of rupture, in C. G. Biezeno and J. M. Burgers, eds., Proceedings of the first International Congress on Applied Mechanics, Tech. Boekhandel en Drukkerij J. Waltman Jr., 54–63.

Holt, R. M., E. Fjaer, O. M. Nes, and H. T. Alassi, 2011, A shaly look at brittleness: Presented at 45th US Rock Mechanics/Geomechanics Symposium, ARMA 11-366.

Hu, Y., M. E. G. Perdomo, K. Wu, Z. Chen, K. Zhang, D. Ji, and H. Zhong, 2015, A novel model of brittleness index for shale gas reservoirs: Confining pressure effect: SPE Asia Pacific Unconventional Resources Conference and Exhibition, SPE-176886.

Jarvie, D. M., R. J. Hill, T. E. Ruble, and R. M. Pollastro, 2007, Unconventional shale-gas systems: The Mississippian Barnett shale of north-central Texas as one model for thermogenic shale-gas assessment: AAPG Bulletin, **91**, 475–499, doi: 10.1306/12190606068.

Jin, X., S. N. Shah, J. C. Roegiers, and B. Zhang, 2015, An integrated petrophysics and geomechanics approach for fracability evaluation in shale reservoirs: SPE Journal, **20**, 518–526, doi: 10.2118/168589-PA.

Kelly, P. A., 2015, Mechanics lecture notes: An introduction to solid mechanics, available from http://homepages.engineering.auckland.ac.nz/~pkel015/SolidMechanicsBooks/index.html

Lutz, S. J., S. Hickman, N. Davatzes, E. Zemach, P. Drakos, and A. R. Tait, 2010, Rock mechanical testing and petrologic analysis in support of well stimulation activities at the desert peak geothermal field, Nevada: Proceedings of the 35th Workshop on Geothermal Reservoir Engineering.

Mathia, E., K. Ratcliffe, and M. Wright, 2016, Brittleness index — A parameter to embrace or avoid? URTeC: 2448745.

McKean, S. H., 2017, Geomechanical properties of the Montney and Sulphur Mountain Formations: M.S. thesis, University of Calgary.

Miller, C., D. Hamilton, S. Sturm, G. Waters, T. Taylor, J. L. Calvez, and M. Singh, 2013, Evaluating the impact of mineralogy, natural fractures and in situ stresses on hydraulically induced fracture system geometry in horizontal shale wells: SPE Hydraulic Fracturing Technology Conference, SPE, 163878.

Miskimins, J. L., 2012, The impact of mechanical stratigraphy on hydraulic fracture growth and design consideration for horizontal wells, Search and Discovery Article #41102, available at http://www.searchanddiscovery.com/documents/2012/41102miskimins/ndx_miskimins.pdf, accessed 11 March 2019.

Ouenes, A., 2014, Distribution of well performances in shale reservoirs and their predictions using the concept of shale capacity: SPE Annual Technical Conference and Exhibition, SPE 167779.

Rickman, R., M. J. Mullen, J. E. Petre, W. V. Grieser, and D. Kundert, 2008, A practical use of shale petrophysics for stimulation design optimization: All shale plays are not clones of the Barnett shale: SPE Annual Technical Conference and Exhibition, SPE 115258.

Rocha-Rangel, E., 2011, Fracture toughness determinations by means of indentation fracture, nanocomposites with unique properties and applications in medicine and industry, J. Cuppoletti, ed., ISBN: 978-953-307-351-4, InTech, available from https://www.intechopen.com/books/nanocomposites-with-unique-properties-and-applications-in-medicine-and-industry/fracture-toughness-determinations-by-means-of-indentation-fracture, accessed 9 March 2019.

Sack, R. A., 1946, Extension of Griffith's theory of rupture to three dimensions: Proceedings of the Physical Society, **58**, 729, doi: 10.1088/0959-5309/58/6/312.

Sharma, R. K., and S. Chopra, 2015, Determination of lithology and brittleness of rocks with a new attribute: The Leading Edge, **34**, 554–564, doi: 10.1190/tle34050554.1.

Sharma, R. K., S. Chopra, H. Nemati, J. Keay, and L. Lines, 2018, Seismic reservoir characterization of Utica-Point Pleasant shale with efforts at fracability evaluation — Part 2: A case study: Interpretation, **6**, no. 2, T325–T336, doi: 10.1190/INT-2017-0135.1.

Sharma, R. K., S. Chopra, and L. R. Lines, 2019, Challenges and uncertainty in the seismic reservoir characterization of Bone Spring and Wolfcamp formations in the Delaware Basin using rock physics: 89th Annual International Meeting of the SEG, Expanded Abstracts, 4928–4932, doi: https://doi.org/10.1190/segam2019-3214084.1.

Sierra, R., M. Tran, and Y. Abousleiman, 2010, Woodford Shale mechanical properties and the impacts of lithofacies: Presented at 44th US Rock Mechanics Symposium and 5th US-Canada Rock Mechanics Symposium, ARMA-10461.

Wang, F. P., and J. F. Gale, 2009, Screening criteria for shale-gas system: Gulf Coast Association of Geological Societies Transactions, **59**, 779–793.

Wang, G., and T. R. Carr, 2012, Methodology of organic rich shale lithofacies identification and prediction: A case study from Marcellus shale in the Appalachian Basin: Computers & Geosciences, **49**, 151–163 doi: 10.1016/j.cageo.2012.07.011.

Yagiz, S., 2009, Assessment of brittleness using rock strength and density with punch penetration test: Tunnelling and Underground Space Technology **24**, 66–74, doi: 10.1016/j.tust.2008.04.002.

You, M., 2011, Strength and damage of marble in ductile failure: Journal of Rock Mechanics and Geotechnical Engineering, **3**, 161–166, doi: 10.3724/SP.J.1235.2011.00161.

Zhang, J. J., and L. R. Bentley, 2005, Factors determining Poisson's ratio: CREWES Research Report, **17**, 1–15.